Automatic Detection of a Subsurface Wire Using an Electromagnetic Gradiometer

Sean P. McKenna, Kevin B. Parkman, Lee J. Perren, and Jason R. McKenna

***Abstract*—A model-based correlation detection scheme is presented with the aim of detecting and localizing subsurface tunnel infrastructure in an automated fashion. Our goal is to develop a comprehensive detection technology that can be fielded and successfully used by non-experts, while simultaneously being sufficiently robust as to be an effective tool. Our correlation detection algorithm relies on a library of model signals that are generated using an analytical model of a thin subsurface wire in a homogeneous half-space. The wire is illuminated using an active transmitter source and its response is sensed using a man-portable electromagnetic gradiometer (EMG) system. The performance of the detector is assessed using synthetic data and receiver operating characteristic (ROC) analysis as well as experimental data collected during a field test. The ROC results indicate that as the signal-to-noise ratio approaches 1.5, the detector performance becomes excellent (probability of detection near 0.99 with a false alarm rate of one every 5200 m). Results from the field tests revealed that the responses from the EMG can be used to detect and localize (to within 0.5 m) a wire target down to a depth of at least 7 m. We feel the EMG system and correlation detector combine to form a promising technology for detecting tunnel infrastructure that can be used by experts and, more importantly, non-experts as well.**

***Index Terms*—Buried object detection, detection algorithms, electromagnetic induction, correlation.**

I. Introduction

CLANDESTINE underground tunnels mark a persistent threat to the borders of the continental United States, serving as conduits for the trafficking of illegal drugs, persons, and weapons. Current methods of successfully identifying potential tunnel locations depend on reliable human intelligence. Many alternative techniques have been applied to the problem over the years, including the use of trained K-9 units and various geophysical methods such as gravity, ground-penetrating radar, electromagnetic (EM), seismic, and synthetic aperture radar methods (e.g., [1]–[4]). Each has met with varying degrees of success. A "silver bullet" method for tunnel detection has yet to be developed and proven. While non-invasive geophysical methods represent the most likely approach, the need for high resolution information, rapid data acquisition, and minimal exposure of field personnel have rendered most methods impractical.

In this paper, we look at automatic target detection with an EM gradiometer (EMG) system that we have been evaluating as one of several tunnel detection technologies. Sensing with the EMG is based on the principles of electromagnetic induction (EMI). The idea behind this method is to illuminate an electrically conductive target below the surface with an oscillating magnetic field. This time-varying field induces currents in the target(s) that radiate secondary magnetic fields, which can produce a detectable response given a suitable sensor. For the application considered here, we are interested in the response of the EMG system to long, linear, underground conductors such as wires, cabling, and railings. Such infrastructure is often found in underground tunnels [5] and can be exploited for detection purposes using such an EMI approach. Similarly, this type of sensor modality can be used to detect surface and shallowly buried wires like those employed in certain types of improvised explosive devices.

The EMG is a frequency-domain system that consists of an active coil transmitter of diameter 0.72 m (usually in a fixed location and oriented as a vertical magnetic dipole) and a mobile sensor (here, man-portable), which uses a pair of receivers that produce a gradiometric measurement (see Fig. 1). An earlier version of the EMG is described in [6] and [7]. The receivers can be oriented either vertically (as shown) or horizontally in order to measure different components of the electromagnetic field. The system is designed to operate with the active transmitter at 4, 12, 20, 80, and 200 kHz. The sensor is outfitted with a GPS unit that yields cm-level position accuracy. The EMG system is an attractive option for subsurface sensing because it can be deployed rapidly, it can be used in a variety of terrains using a number of different mounting options (e.g., the system can be vehicle-mounted), it does not require permanent or costly installation, and it can cover relatively large amounts of territory within a short timeframe.

Thus far, detection of subsurface conductors with the EMG has been limited to "back office" post-processing and analysis by skilled analysts. This is true of the majority of sensor technologies fielded today. To be truly effective in an operational sense, detection needs to be done in near-real-time without the need for highly experienced or knowledgeable field personnel. This paper describes an automatic target detection approach that exploits the data from the EMG using a GUI-based field application. In addition to performing detection, the tool we have developed provides a user-friendly visualization framework for working with survey data collected with the EMG. The visualization component is designed to read in EMG data files, do some basic data quality control and manipulation, and then display the data in both timeseries and geospatial formats for quick inspection and analysis.

Our approach to developing an automatic detection capability relies on a model-based correlation scheme. The model

S. P. McKenna, K. B. Parkman and J. R. McKenna are with the U.S. Army Engineer Research and Development Center, Vicksburg, MS 39180 USA (e-mail: sean.p.mckenna@usace.army.mil).

L. J. Perren is with Bevilacqua Research Corporation, Huntsville, AL 35805 USA.

Manuscript received Month Day, 2011.

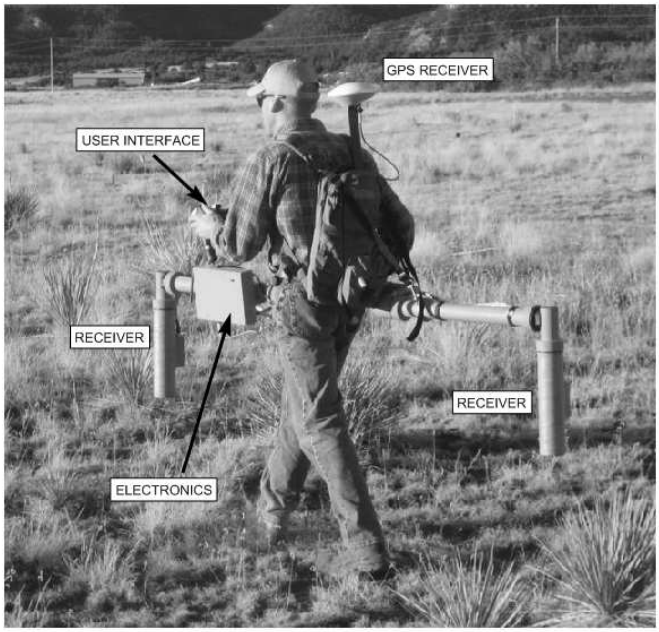

Fig. 1. Photograph of the man-portable electromagnetic gradiometer sensor.

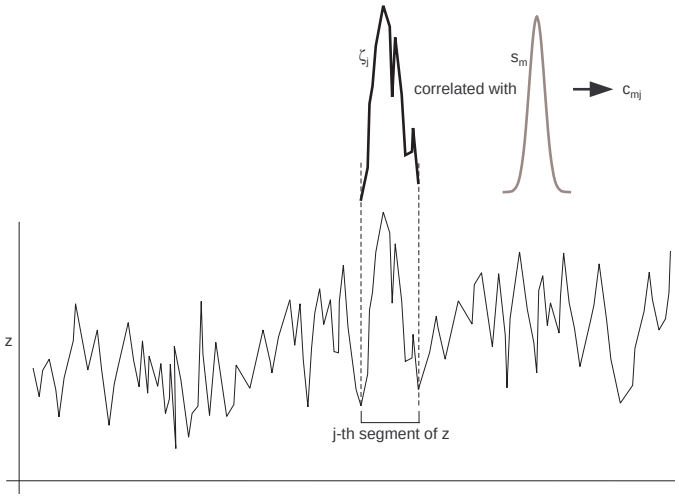

Fig. 2. Illustration of the correlation process. The complete data series is subdivided into smaller segments using a sliding window approach. Each segment of data, ζ_j, is then cross-correlated with each of the M hypothesized signals (s_m) to yield a matrix of correlation coefficients c_{mj}.

that forms the basis for the correlator has been discussed in detail in [8]. Furthermore, the model has been compared to experimental results, showing favorable agreement in [9]. Relevant details of the model are included in section II. While there are other methodologies for detection that may be more sophisticated (e.g., wavelet schemes [10], principal component analyses [11], neural networks [12], support vector machines [13], and others), a correlation scheme was chosen because it is straightforward yet robust, intuitively attractive, and requires very little to implement and execute. A correlation technique similar to that employed here has been used for buried target detection by [14].

This paper is organized as follows. Section II describes our correlation detection approach and implementation and provides an initial assessment of its behavior using synthetic data. In Section III, we present results and analysis from a field experiment where field performance of the correlation detector was assessed. Section IV offers our conclusions.

II. Correlation Detection Approach

In signal detection theory, the optimum scheme for detecting a known signal corrupted by additive white noise is through the operation of correlation [15]. The correlation of two signals is a measure of similarity between the two sequences. The essence of the correlator detection algorithm we have developed is to subdivide the survey data series into smaller segments and assess the degree of match between prescribed model signals and each segment. The methodology resembles template matching and is closely related to the technique of matched filtering [16].

As eluded to above, a correlation-based approach was selected for its relative simplicity and its ease of implementation. Furthermore, the algorithm can be configured to require only a single user input, which was highly desirable since minimizing user inputs was a key requirement for our fieldable system. (Again, one must keep in mind that this tool is intended for field deployment and use by non-experts.)

Another benefit to the correlation approach is that it can be designed in such a way so as to allow multiple detections along a given survey line (i.e., free-response behavior). And lastly, it can provide target localization. These last two features are important since we are not simply interested in whether or not a target (or at least one target) is detected along a survey line. Rather, we are interested in all potential targets and their precise locations along a survey line.

A. Mathematical basis

We begin by defining the following set of hypotheses:

$$\begin{aligned} H_0 &: \zeta_j = n \\ H_1 &: \zeta_j = s_1 + n \\ &\vdots \quad \vdots \\ H_M &: \zeta_j = s_M + n, \end{aligned} \tag{1}$$

where each s_m ($m = 1 \ldots M$) represents a hypothesized target signal, and ζ_j is the sequence of points contained in the j-th segment of z, where z is the measured data (refer to Fig. 2). In our case, z corresponds to the magnitude of the EMI gradient response measured by the EMG. This set of hypotheses consists of the hypothesis that the data segment is noise, along with a suite of hypotheses that state that the data segment is signal plus noise. The hypotheses in (1) are considered independently for each ζ_j segment along the complete data series. The approach is to determine, for each segment of data, which of these hypotheses is most likely true. To do that, we use a cross-correlation approach. For each data segment, the normalized correlation coefficient between it and each target signal is computed:

$$c_{mj} = \frac{E[(\zeta_j - \mu_{\zeta_j})(s_m - \mu_{s_m})]}{\sigma_{\zeta_j}\sigma_{s_m}}, \tag{2}$$

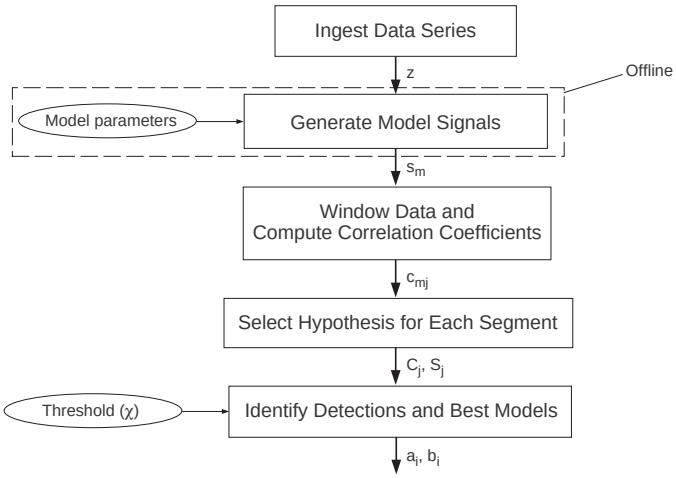

Fig. 3. Flow chart for the correlator detector.

where μ_{ζ_j} and μ_{s_m} are the means of ζ_j and s_m, respectively, σ_{ζ_j} and σ_{s_m} are their standard deviations, and $E[\ ]$ is the expectation operator. The coefficient c_{mj} will range from -1 to 1, the former signifying perfect anti-correlation, the latter signifying perfect correlation. If ζ_j and s_m are uncorrelated, or statistically independent, $c_{mj} = 0$. Using this measure of correlation, we can select the signal-plus-noise hypothesis that best matches the data in each segment. This, by itself, is not sufficient for target detection. A simple threshold technique is then used to assess whether or not the degree of match is sufficient to choose one of the signal-to-noise hypotheses and consequently declare a target detection. Otherwise, the noise-only hypothesis is chosen (no target present).

B. Detector Design and Operation

The correlation approach outlined in the previous section was automated in MATLAB and used as the basis for a correlator detection scheme. Fig. 3 outlines the operation of the correlator detector. Details of each of the stages of the detector are given in the sections that follow. From a user point of view, data is loaded into the application, selected for detection, optional parameters can be set, a single required parameter is set, and a button press executes the detection algorithm automatically. Results can be viewed graphically or exported to a text file or a Google Earth kml file.

1) Model signal generation: The correlator scheme requires models for the hypothesized target signals. The model signals may be determined in a variety of ways, including physical modeling, parameterizations or empirical approaches, or from real sensor data. For the detector discussed here, we utilize a model library that is populated by running our analytical model over a parametric sweep of relevant parameters. The model is a fully analytical model for a frequency-domain EMI sensor over a homogeneous earth containing a long linear conductor [8]. The model determines the total field as it would be sensed by a receiver coil at an arbitrary location above the earth, i.e., the combination of the primary field due to the transmitter, the field due to the presence of the earth, and the field from the buried linear conductor. The model is based on an integral transform approach (e.g., [17], [18]) for a vertical magnetic dipole source and a receiver that can measure the three components of the magnetic field. We have implemented the model in the MATLAB computing environment, enabling us to simulate target responses under a wide variety of conditions.

In our model, the magnetic field measured at a receiver is assumed to be composed of the following:

- Fields due to the dipole source: $\mathbf{H}^d = \mathbf{H}^{d,p} + \mathbf{H}^{d,s}$ [19], where the primary field is denoted with the superscript 'p' and the secondary field is denoted with an 's'. The primary field is the field in the absence of the conducting earth. The secondary field is that which results from the presence of the conducting earth.
- Field due to the presence of a linear subsurface conductor at constant depth: $\mathbf{H}^c$. The conductor field is determined from three main steps—(1) the electric field incident on the buried conductor is computed for a homogeneous half-space, taking into account the presence of the air–earth interface, (2) the current in the conductor is determined using the incident electric field and a specified axial impedance condition for the conductor in the earth, and (3) the radiated field due to the induced current in the buried conductor is computed for a homogeneous half-space, taking into account the presence of the air–earth interface.

The model assumes that the total magnetic field measured at a receiver is given by a superposition of the dipole fields (primary and secondary) and the conductor field,

$$\mathbf{H} = \mathbf{H}^d + \mathbf{H}^c = \mathbf{H}^{d,p} + \mathbf{H}^{d,s} + \mathbf{H}^c. \tag{3}$$

For the analysis presented in this paper, a single library was considered (see Table I for the library parameters), although we have a number of other libraries that we have generated to cover other survey/target conditions and scenarios. (Similar library-based approaches to detection of buried targets are described in [20], [21], and [22].) This particular library contains 14,175 model signals. In order to reduce this large number of potential model signals (and speed up the detector), the user has the ability to bound the ground conductivity and the expected target depth if possible. Furthermore, only a single value of y_s is used since it is straightforwardly computed based on the positions of the transmitter and the survey line. Lastly, for this library, the survey line crosses the target wire orthogonally.

Generation of the thousands of model signals is a time-consuming step and is done offline; however, using a library of analytical models has the benefit of enabling the detector to provide preliminary target identification information when reporting a detection (e.g., target depth and orientation).

2) Data windowing and correlation calculation: Windowing the data z to yield the ζ_j segments is done using a sliding window approach. The window is moved point by point, and the number of segments is simply a function of the length of z and the window size. The number of points in the segments is governed by the physical width of the widest model signal and the mean spatial sampling rate. The correlation between

TABLE I
MODEL LIBRARY PARAMETERS

Ground conductivity (mS/m)	Wire depth (m)	Frequency (kHz)	y_s [a] (m)	x_{TX} [a] (m)
0.1	2	20	20	-20
1	3	80	30	-10
10	4	200	40	-5
50	5	500	50	0.1
100	6	800	60	5
	7		70	10
	8		80	20
	9		90	
	10		100	

[a] Parameters y_s and x_{TX} are explained in Fig. 8.

the data segment and each model signal is computed using (2). Note, since the coefficient in (2) is variance-normalized, the amplitude of the model signal is arbitrary. The result is a matrix of coefficients where each row corresponds to a signal model and each column corresponds to a data segment (the c_{mj} matrix).

3) Select hypothesis for each segment: To determine which signal-plus-noise hypothesis best matches the data for each segment, the maximum values are taken along the columns of the correlation coefficient matrix. These will be denoted C_j (see Fig. 4). The models corresponding to these maximums represent the best matching models to the data in each segment. These models will be denoted S_j. The final step is to decide whether a signal-plus-noise hypothesis is chosen over the noise-only hypothesis. This decision is made using a simple threshold test. Setting a correlation coefficient threshold, χ, the threshold test is:

$$\text{if } C_j \geq \chi, \tag{4}$$

then we chose the signal-plus-noise hypothesis corresponding to S_j and we have a detection in the j-th data segment. Otherwise, we choose the noise-only hypothesis. The threshold χ is the sole input parameter required of the user.

4) Estimating anomaly location: To determine the position of the i-th detection, we first select the index of the peak value in the cluster of points (or single point) exceeding the set threshold. For instance, in Fig. 4, there are eight C_j that exceed the set threshold; however, they all correspond to the same detection. This peak point corresponds to the best model match (denoted b_i). The peak of the correlation result from this model is then used in a three-point Gaussian curve fit to more precisely (a fractional index) locate the position of the detection (denoted a_i).

5) Additional considerations: Operationally, a given survey line is typically surveyed twice, once in each direction. The detector has the option to process this dual-pass information to improve its localization accuracy. Specifically, if a detection exists on one survey track and there is a detection on the opposing track within a certain "merging distance," the two detections are combined via simple averaging. Lastly, the EMG has the ability to collect data at multiple frequencies simultaneously. If multi-frequency data is collected, the detector is designed to handle such data using user-specified weights for each frequency and combining the individual correlation results using a Fisher z-transform approach.

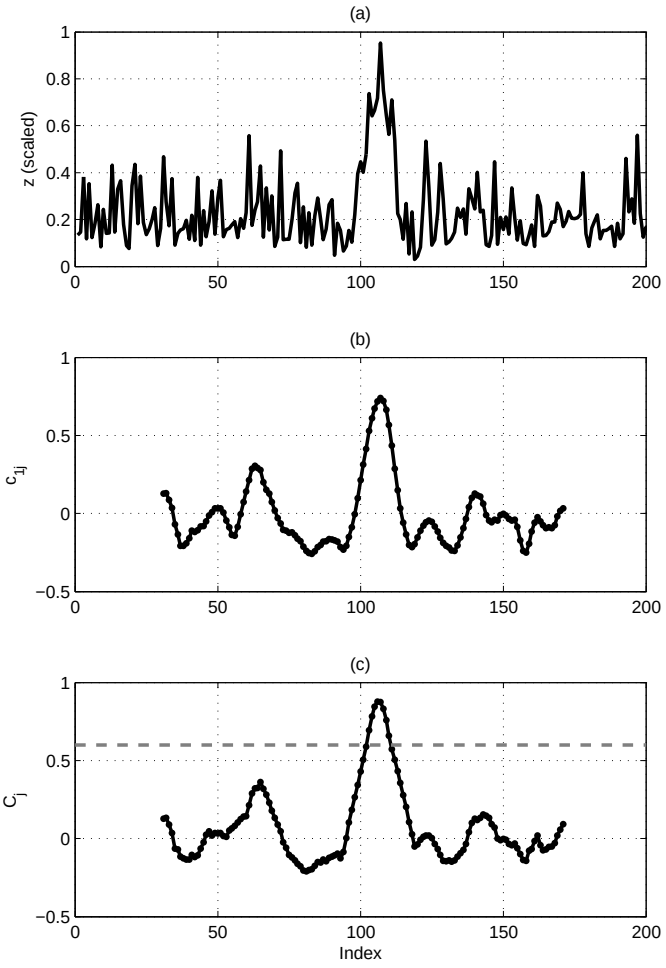

Fig. 4. Example of correlator detector steps. (a) The data z (scaled) with a single target anomaly at index = 106 (SNR = 1.5); (b) the correlation result c_{1j} for hypothesis H_1; (c) the C_j result with $\chi = 0.6$ indicated as the dashed gray line—above the gray line, a signal-plus-noise hypothesis is selected, below the gray line, the noise-only hypothesis is selected.

C. Detector Behavior

In order to gain an fundamental sense of the correlator detector performance, a receiver operating characteristic (ROC) analysis was conducted. To compute the ROC, a Monte Carlo approach using synthetic data was used. For each Monte Carlo survey trial, a single target is prescribed. Then, for each survey trial:

- If no detections are made, neither a correct detection nor a false alarm is declared.
- If at least one detection is made, the distance to the detection closest to the true target is computed.
- If this distance is within a specified localization accuracy threshold, a correct detection is declared. All other detections, if any, are counted as false alarms.
- If the distance is outside the detection accuracy threshold, a false alarm is declared. All other detections, if any, are

counted as additional false alarms.

The synthetic data consisted of a single reference target randomly located along a 100-m long survey with additive noise. (For each Monte Carlo run, the target was relocated randomly.) The reference target corresponded to a thin copper wire buried in a 10-mS/m ground at a depth of 5 m sensed using a system frequency of 200 kHz. At this stage, our understanding of the measured noise is limited, therefore, the target signal was corrupted by adding random normally-distributed noise to each receiver's inphase and quadrature components. From these components, we then computed the magnitude of the "measured" gradient response. To gain a sense of detector performance under different levels of additive noise, we specified several signal-to-noise (SNR) ratios to study. The SNR was defined as the ratio of the area under the target signal to the area under the noise signal along the extent of the target signal. Varying the SNR has the effect of studying different target depths. (Note, this statement is not precisely true since in addition to amplitude attenuation with lower SNR, the target signal also widens.) Fig. 5 shows two example synthetic data series, one at an SNR of 0.5 and a second at an SNR of 1.5. Lastly, the survey sample spacing was 0.5 m, and a localization accuracy criterion of ± 0.5 m was used. The latter value was selected based on the typical size of the tunnels we are seeking to discover.

Fig. 6 is the set of ROC curves for the conditions considered. Each point in the figure corresponds to a different χ threshold level. For each SNR level, the ROC curve ramps up to a constant value. At an SNR $= 1$, the detector can achieve a probability of a correctly localized target equal to 0.87 with a false alarm rate of 0.2 per 100 m, or equivalently, one false alarm every 500 m. Below an SNR $= 1$, detector performance falls off below acceptable levels. As the SNR approaches 1.5, the detector performance becomes impressive (probability of detection near 0.99 with a false alarm rate of one every 5200 m).

Study of the ROC curves and user experience indicates a threshold $\chi = 0.6$ provides a good balance between detection performance and false alarm density. There are cases, however, when a trial-and-error approach is needed to best determine the most effective value of χ.

III. Experimental Field Study

Using data that was collected with the EMG at a dedicated test site in the southwestern United States, we were able to gain an initial assessment of the detector performance in a field setting. The site consisted of a horizontally drilled borehole whose depth profile is given in Fig. 7. The borehole contained a 7.6 cm-diameter PVC pipe, inside of which was a 18 AWG shielded twisted pair wire. The wire was grounded to the earth at both ends of the borehole.

Six survey lines were used, and a number of transmitter locations were explored (see Fig. 8). Table II presents the details of each survey line: the survey line number, the survey line distance (y_s), the angle at which the survey line crosses the conductor (0° corresponds to perfectly orthogonal), and the depth of the conductor at each survey line. The transmitter was

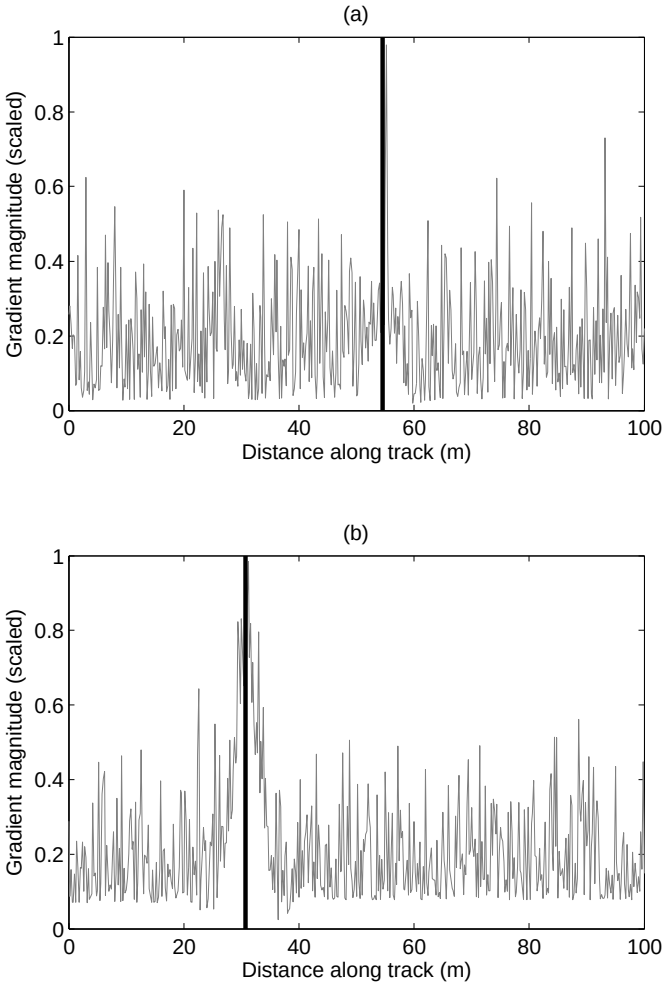

Fig. 5. Example synthetic data series: (a) SNR = 0.5, (b) SNR = 1.5. The vertical black lines indicate the location of the target along the survey track.

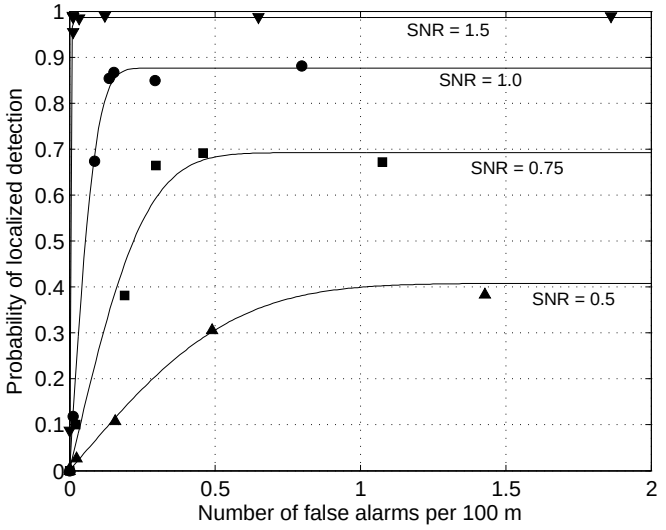

Fig. 6. ROC curves for the four SNRs studied. Points are the raw output from the Monte Carlo analysis. The localization criterion is ± 0.5 m.

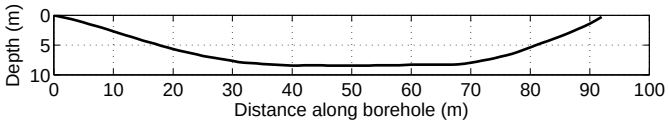

Fig. 7. Borehole depth profile.

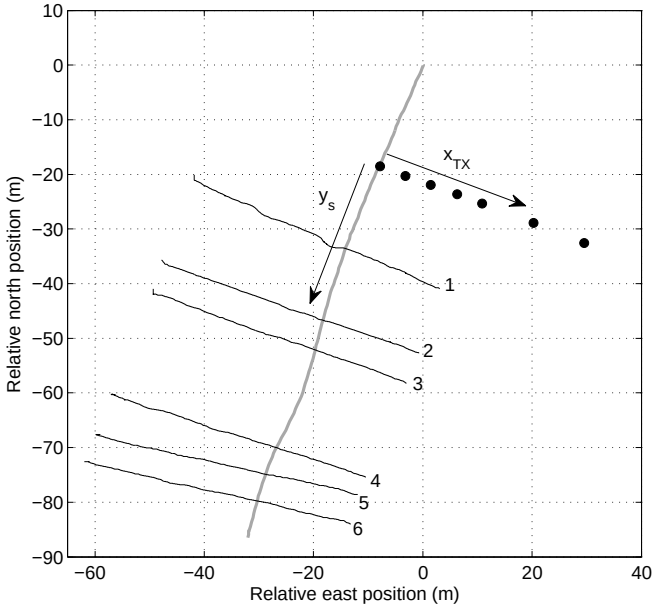

Fig. 8. Experimental survey layout. The grey line represents the buried conductor, the enumerated black lines are the survey tracks, and the circles indicate transmitter positions. Coordinate x_{TX} measures the lateral offset of the transmitter from the conductor axis. Coordinate y_s measures the along-conductor distance to each survey track, starting from the line of transmitter positions.

TABLE II
SURVEY LINE DETAILS

No.	y_s (m)	angle (°)	depth (m)
1	16.5	−0.2	8.3
2	30.2	−2.5	8.5
3	35.7	−3.5	8.4
4	55.0	6.1	7.0
5	60.2	7.9	5.3
6	65.3	4.9	3.4

positioned at the following values of x_{TX}: 0, 5, 10, 15, 20, 30, and 40 m. The transmitter was laid on the ground surface (vertical magnetic dipole orientation) and operated at 200 kHz (12 and 20 kHz were also used; these are discussed later). Each survey line was roughly 50 m in length, and measurements were made in both directions along the line, west-to-east and east-to-west. Directional repeatability was very good overall, and in some cases the repeatability was remarkable.

Fig. 9 shows a sample of the experimental results for survey tracks 4, 5, and 6 at a frequency of 200 kHz. The other three lines (those closest to the transmitter) suffered from transmitter signal influence ([9]) and could not be used to evaluate the detector performance. The figure provides a sense of how the gradient magnitude response is affected by the target

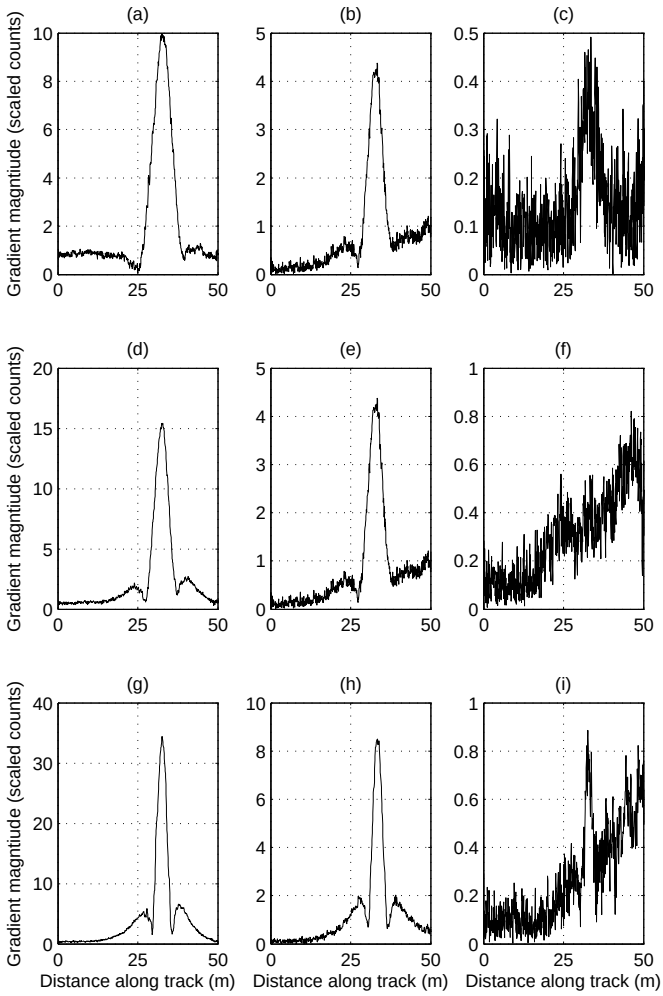

Fig. 9. Selection of 200-kHz experimental data. Top row: track 4, middle row: track 5, bottom row: track 6. Left column: $x_{TX} = 10$ m, middle column: $x_{TX} = 20$ m, right column: $x_{TX} = 40$ m. Tracks are west to east, and the target is located approximately 33 m along the track.

depth (i.e., the track number) and the transmitter offset (x_{TX}). Deeper targets produce wider responses, shallower targets produce narrower. Also, as the transmitter is increasingly offset from the target, the response becomes more noisy. Clearly, there are cases where the SNR is extremely high. There are also some cases, where the SNR is more akin to that shown in Fig. 5.

If we run our detector tool on the data in Fig. 9 in dual-pass mode (i.e., both west-to-east and east-to-west passes are used), we obtain the results shown in Fig. 10, which is a Google Earth screen capture. Providing the user the ability to export their results to Google Earth is a powerful feature that enables easy and consistent visualization of the detection output. As can be seen from the figure, eight detections were made—a successful detection was not made for the data in Fig. 9f. Localization errors ranged from 3 cm to 22 cm with a mean value of 10.5 cm. The detection that is expanded in the Google Earth Places pane indicates an estimated target depth of 7.5 m. This value is based on the best matching model that was selected for the detection. The true depth of the target at

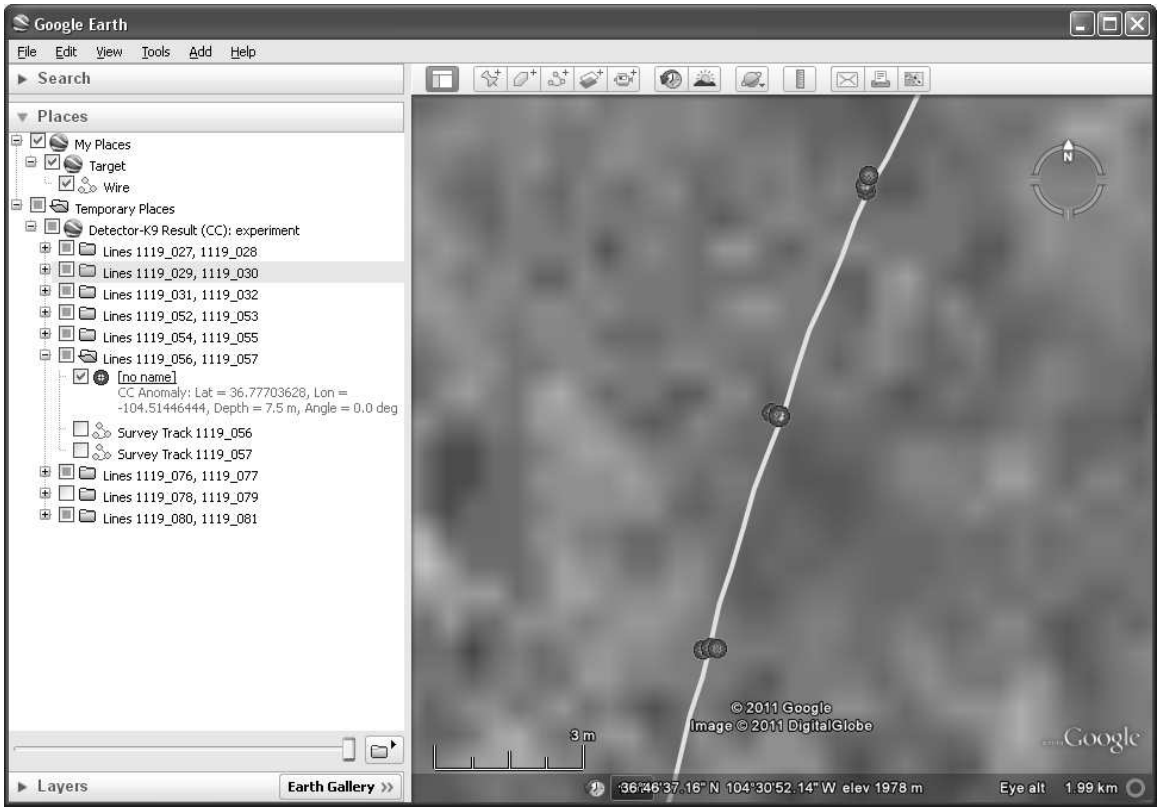

Fig. 10. Google Earth display of the detector output. The detections are indicated by the circular icons and the subsurface wire is shown by the solid line. The northernmost points correspond to survey track 4, the middle points correspond to survey track 5, and the southernmost points correspond to survey track 6. To the left are each of the dual-pass detections with one detection (one of the northernmost) expanded to show more detail (geodetic position, estimated depth and orientation angle).

this location, 7 m, is quite close to the detector estimate.

For a more comprehensive assessment of the detector, we looked at all of the usable data collected during the field experiment. This amounted to 86 dual-pass survey lines at 12, 20, and 200 kHz. In some cases, no target was present (i.e., the wire was removed). In a handful of cases, the wire was traversed at an angle. We also note that the data collected at 12 and 20 kHz was much noisier than the data at 200 kHz, and this was reflected in the detector perfromance at these two frequencies. The resulting confusion matrix for all the available data is given in Fig. 11. We found a probability of detection of 0.966 and a false alarm rate of 0.140 per 100 m. The latter is equivalent to a single false alarm every 717 m. The six false alarms were all due to incorrect localization of detections and the errors in localization ranged from 0.60 to 1.77 m (three were 0.64 m or less). There were no extraneous detections (type I errors).

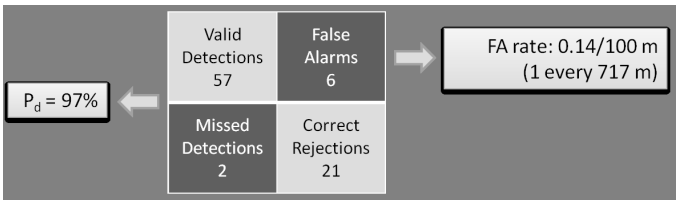

Fig. 11. Confusion matrix for all usable experimental field results. Data was processed in the dual-pass mode with $\chi = 0.6$ throughout. The localization criterion is ± 0.5 m.

IV. Conclusion

Subsurface tunnel detection continues to be a challenging problem, and in particular, (near-)real-time detection. Furthermore, in many instances, users of any particular detection system will not be experts in near-surface geophysics, the specific technology being used, or detection theory. It therefore becomes imperative that any system deployed to the field be designed to be as simple to use and automated as practical. This paper has presented an EMG system that, when coupled with our model-based detector, serves as a straightforward technology capable of tunnel detection and localization.

Our ROC results using synthetic data showed that for SNR values of unity of greater, the detector performance is able to meet desired specifications. Field tests confirmed that the detector is able to successfully detect and localize a buried wire target at depths up to 7 m. Noteworthy is the fact that the detector showed robust performance given a single user parameter that was fixed for the analysis. This is in contrast to more sophisticated detection schemes that require far more adjustable parameters. Overall, we feel the EMG system and correlation detector combine to form a promising technology for detection tunnel infrastructure. At the very least, this system can provide a useful first pass detection capability that can be augmented with additional sensors and systems to increase detection success.

It should be noted that the field testing was under relatively benign experimental conditions. Realized SNR values were generally quite high, especially for the 200-kHz data and for the shallow target depths. Future field testing will have to be done under more challenging conditions, e.g., deeper targets, clutter present. Further testing of the EMG system and correlation detection under such conditions will serve to better quantify its expected performance in more realistic field settings.

ACKNOWLEDGMENT

Funding for this research was provided by the U.S. Army Engineer Research and Development Center under the Rapid Reaction Tunnel Detection Program. The Director, Geotechnical and Structures Laboratory, U.S. Army Engineer Research and Development Center granted permission to publish.

REFERENCES

[1] D. K. Butler, "Microgravimetric and gravity gradient techniques for detection of subsurface cavities," *Geophysics*, vol. 49, no. 7, pp. 1084–1096, Jul. 1984.

[2] T. Counts, G. Larson, A. C. Gürbüz, J. H. McClellan, and W. R. Scott, Jr., "Investigation of the detection of shallow tunnels using electromagnetic and seismic waves," in *Proc. SPIE*, vol. 6553, May 2007.

[3] R. Miller, C. B. Park, J. Xia, J. Ivanov, D. W. Steeples, N. Ryden, R. F. Ballard, J. L. Llopis, T. S. Anderson, M. L. Moran, and S. A. Ketcham, "Tunnel Detection Using Seismic Methods," in *Proc. AGU Meeting*, Baltimore, MD, May 2006, NS21A-07.

[4] J. A. Martinez-Lorenzo, C. M. Rappaport, and F. Quivira, "Physical limitations on detecting tunnels using underground-focusing spotlight synthetic aperture radar," *IEEE Trans. Geosci. Remote Sens.*, vol. 49, no. 1, pp. 65–70, Jan. 2011.

[5] K. D. Mahrer and D. F. List, "Radio frequency electromagnetic tunnel detection and delineation at the Otay Mesa site," *Geophysics*, vol. 60, no. 2, Mar./Apr. 1995.

[6] L. G. Stolarczyk, R. Troublefield, and J. Battis, "Detection of underground tunnels with a synchronized electromagnetic wave gradiometer," in *Sensors, and Command, Control, Communications, and Intelligence (C3I) Technologies for Homeland Security and Homeland Defense IV*, vol. 5778, no. II. SPIE, May 2005, pp. 994–1001.

[7] L. C. Bartel, D. H. Cress, and L. G. Stolarczyk, "Evaluation of the electromagnetic gradiometer concept for detection of underground structures—theory and application," *Journal of Environmental and Engineering Geophysics*, vol. 2, no. 2, pp. 127–136, Sep. 1997.

[8] S. P. McKenna and J. R. McKenna, "Modeling and analysis of the response of a triaxial, frequency-domain electromagnetic induction sensor to a buried, linear conductor," *Geophysics*, vol. 75, no. 1, pp. F1–F14, Jan./Feb. 2010.

[9] S. P. McKenna, K. B. Parkman, L. J. Perren, and J. R. McKenna, "Response of an electromagnetic gradiometer to a subsurface wire," *IEEE Trans. Geosci. Remote Sens.*, vol. 49, no. 11, pp. 1–10, Nov. 2011.

[10] D. Carevic, "Wavelet-based method for detection of shallowly buried objects from GPR data," in *Information, Decision and Control, 1999. IDC 99. Proceedings. 1999*, Feb. 1999, pp. 201–206.

[11] G. Kaplan, O. Icoglu, A. Yoldemir, and M. Sezgin, "Real-time object detection using dynamic principal component analysis," in *2010 13th International Conference on Ground Penetrating Radar (GPR)*, Jun. 2010, pp. 1–6.

[12] S. Caorsi and G. Cevini, "An electromagnetic approach based on neural networks for the GPR investigation of buried cylinders," *IEEE Geosci. Remote Sens. Letters*, vol. 2, no. 1, pp. 3–7, Jan. 2005.

[13] E. Bermani, A. Boni, S. Caorsi, and A. Massa, "An innovative real-time technique for buried object detection," *IEEE Trans. Geosci. Remote Sens.*, vol. 41, no. 4, pp. 927–931, Apr. 2003.

[14] G. A. Ellis and I. C. Peden, "Cross-borehole sensing: Identification and localization of underground tunnels in the presence of a horizontal stratification," *IEEE Trans. Geosci. Remote Sens.*, vol. 35, no. 3, pp. 756–761, May 1997.

[15] B. V. K. V. Kumar, A. Mahalanobis, and R. D. Juday, *Correlation pattern recognition*. Cambridge University Press, 2005.

[16] A. D. Whalen, *Detection of Signals in Noise*. Academic Press, 1971.

[17] K. Tsubota and J. R. Wait, "The frequency and the time-domain responses of a buried axial conductor," *Geophysics*, vol. 45, no. 5, May 1980.

[18] D. A. Hill, "Magnetic dipole excitation of a long conductor in a lossy medium," *IEEE Trans. Geosci. Remote Sens.*, vol. 26, no. 6, pp. 720–725, Nov. 1988.

[19] J. R. Wait, "Mutual electromagnetic coupling of loops over a homogeneous ground," *Geophysics*, vol. 20, no. 3, pp. 630–637, Jul. 1955.

[20] L. Pasion, S. Billings, D. Oldenburg, and S. Walker, "Application of a library based method to time domain electromagnetic data for the identification of unexploded ordnance," *J. Appl. Geophys.*, vol. 61, no. 3/4, pp. 279–291, Mar. 2007.

[21] S. J. Norton and I. J. Won, "Identification of buried unexploded ordnance from broadband electromagnetic induction data," *IEEE Trans. Geosci. Remote Sens.*, vol. 39, no. 10, pp. 2253–2261, Oct. 2001.

[22] W. Hu, S. L. Tantum, and L. M. Collins, "Emi-based classification of multiple closely spaced subsurface objects via independent component analysis," *IEEE Trans. Geosci. Remote Sens.*, vol. 42, no. 11, pp. 2544–2554, Nov. 2004.